Simulation of Water Transport through a Lipid Membrane

Siewert-Jan Marrink and Herman J. C. Berendsen*

BIOSON Research Institute and Laboratory of Biophysical Chemistry, University of Groningen, Nijenborgh 4, 9747 AG Groningen, The Netherlands

Received: October 22, 1993; In Final Form: January 11, 1994®

To obtain insight in the process of water permeation through a lipid membrane, we performed molecular dynamics simulations on a phospholipid (DPPC)/water system with atomic detail. Since the actual process of permeation is too slow to be studied directly, we deduced the permeation rate indirectly via computation of the free energy and diffusion rate profiles of a water molecule across the bilayer. We conclude that the permeation of water through a lipid membrane cannot be described adequately by a simple homogeneous solubility–diffusion model. Both the excess free energy and the diffusion rate strongly depend on the position in the membrane, as a result from the inhomogeneous nature of the membrane. The calculated excess free energy profile has a shallow slope and a maximum height of 26 kJ/mol. The diffusion rate is highest in the middle of the membrane where the lipid density is low. In the interfacial region almost all water molecules are bound by the lipid headgroups, and the diffusion turns out to be 1 order of magnitude smaller. The total transport process is essentially determined by the free energy barrier. The rate-limiting step is the permeation through the dense part of the lipid tails, where the resistance is highest. We found a permeation rate of $7(\pm 3) \times 10^{-2}$ cm/s at 350 K, comparable to experimental values for DPPC membranes, if corrected for the temperature of the simulation. Taking the inhomogeneity of the membrane into account, we define a new "four-region" model which seems to be more realistic than the "two-phase" solubility–diffusion model.

1. Introduction

A. Biological Relevance. The transport of small molecules across lipid membranes is a biological process of great importance. The regulation of ion concentration inside and outside cells, for instance, is the key process in the functioning of almost every cell. Most biologically significant transport processes across membranes involve the help of some regulatory mechanism. Without special proteins it would almost be impossible for a charged molecule to pass the hydrophobic interior of cell membranes. Small, uncharged molecules (e.g., water, oxygen, formamide, urea), however, permeate the membrane via a basal pathway, i.e., without any regulatory mechanism, at an appreciable rate.[1] Even in the presence of channels, the major route of water permeation through plasma membranes seems to be through the lipid bilayer.[2] Thus, the basal permeation has a general role to establish osmotic balance. In some cases the basal permeation also has a specific biological role.[3,4]

B. Goal of Simulations. Insight into the basal permeation process will enhance the understanding of membranes in general and their interaction with small molecules in particular. The details of the basal permeability are still open for discussion. From section 2 it will become clear that a more realistic model for the permeation process is needed, which takes into account more of the local details of the membrane.

The goal of our research is to elucidate the molecular mechanism underlying the transport of small molecules across a lipid membrane in order to determine which details are important for the permeation process. Therefore, we decided to perform molecular dynamics (MD) simulations of a phospholipid/water bilayer system and to study the permeation process of water as a starting point. Other penetrants are currently being studied. One of the advantages of MD is that it enables investigation of the problem at the atomic level. This is, in the case of membranes, not possible by means of experimental techniques. A disadvantage is the limited time scale available to simulations of such large systems. Whereas on an experimentally accessible time scale (seconds) the number of water molecules that cross the membrane is on the order of a million/nm^2, this number drops far below one on the accessible MD time scale (nanoseconds). It is therefore not possible to study the permeation of water molecules directly in a statistically significant way. The molecular dynamics technique, however, provides an indirect way to do this simply by forcing the water molecules to reside in the membrane. In this way the behavior of water at various positions in the membrane can be examined. In order to get a more detailed description of the permeation process, we derived an equation for the permeation rate, in which both the diffusion and the solubility of a water molecule are position dependent. The computed permeation rate can then be compared to the experimental values.

Apart from the permeability coefficient, the MD simulations should be able to answer the following questions: How do the free energy and diffusion rate of a water molecule depend on the position within the membrane? How large is the influence of the interface? What is the rate-limiting step in the permeation process? What is the type of the diffusion process? Does the membrane resemble a soft polymer or a liquid alkane, neither, or perhaps both? How is the free volume distributed? Where does the size selectivity occur? In general, is a homogeneous solubility–diffusion model really an adequate description of the permeation process? As far as we know, the presently reported simulations are the first to study the total permeation process through lipid membranes. Related studies involve the recent nonequilibrium MD study[5] of oxygen diffusion through a simple hexadecane model membrane, focusing on the cholesterol dependence of the permeation rate, and MD simulations[6] of a benzene molecule in a lipid bilayer, focusing on the diffusion mechanism. As stated above, our goal is to understand the total permeation process through a lipid bilayer.

The simulations we present here are an extension of our previous simulations of a phospholipid membrane in the liquid-crystalline phase.[7,8] The goal of these simulations was to develop a stable membrane that could serve as a model for a biological membrane. A thorough comparison with available experimental data (e.g., tail order parameters, atom distributions, area per headgroup, electron density, fraction of gauche angles) convinced us of the reliability of these simulations.

* Abstract published in *Advance ACS Abstracts*, February 15, 1994.

0022-3654/94/2098-4155$04.50/0

C. Experimental Measurements. Experimental permeation rates of small molecules can be measured by means of osmotic, NMR, and radio-tracer experiments, although the interpretation of the results is often difficult. Unstirred layer effects and different estimations of membrane area and volume are the main causes of the large spread in reported permeation rates. Also, many experiments are done on biological membranes with proteins and peptides embedded, so additional problems arise in blocking the nonbasal permeation pathways. As a consequence, the range of reported experimental values is rather broad. Furthermore, the values will naturally depend on the type of membrane and on temperature. For the permeability coefficient of water, osmotic measurements of unilamellar DPPC vesicles yield a value of 6.32×10^{-4} cm/s at 315 K[9] and of 1.7×10^{-3} cm/s at 317 K.[10] Osmotic measurements on black film DPPC membranes give a value of 3.15×10^{-3} cm/s at 310 K.[11] For permeation across EggPC membranes values of 4.2×10^{-3} cm/s at 309 K,[12] $(7–10) \times 10^{-3}$ cm/s at 309 K,[13] and 3.7×10^{-3} cm/s at 298 K[14] have been reported, all by means of osmotic flow through black films. The basal permeability of water through the red blood cell (RBC) membrane has been investigated more thoroughly. In a recent review all values were brought together and converted to a standard "cell" and temperature, resulting in a quite accurate value for the permeability. The mean value is reported to be 8.1×10^{-3} cm/s at 315 K.[15] Across various other eukaryotic cells, basal permeability rates are usually reported in the range $10^{-3}–10^{-2}$ cm/s.[4,16–20]

D. Outline. In the next section, we review the existing models of the permeation process through lipid membranes. Then we give a theoretical derivation of the permeation process which relates to properties that can be computed from the MD simulations. Section 4 gives details of the simulations and the methods to calculate the permeability coefficient from the position-dependent diffusion and free energy data, as well as some remarks about the computation of radial distribution functions and free volume distributions. Thereafter, the results of the simulations and their interpretation are given, followed by a discussion of the permeation process. Finally, the main conclusions are summarized.

2. Permeation Models

A. Homogeneous Solubility–Diffusion Model. The observed permeation rates are often qualitatively explained by means of a homogeneous solubility–diffusion model,[21–23] which originally was developed to describe penetrant permeation through polymer membranes.[24] In this model the permeation is described as a three-stage process: first, the molecule has to dissolve into the membrane, then has to diffuse through the membrane interior, and finally has to dissolve again in the surrounding phase. The permeation of small molecules across polymer membranes can be explained very well by this mechanism. When applied to lipid membranes, the membrane is being regarded as a homogeneous phase resembling liquid alkanes with well-defined boundaries, separating it from the water phase. In the case of water permeation, using the solubility and diffusion values in hexadecane, the calculated permeation rate lies within the experimental range of reported values.[12] Because this model is simple and works so well (even quantitatively) in the case of water permeation, it has been widely used also to describe the permeation process of other molecules across the membrane.

However, a few remarks should be made. First, thus far it has been impossible to measure either the penetration step or the diffusion step directly in a lipid membrane. This means that only the total predicted permeation rate can be compared with the experimental results. Besides, the range of experimental values is broad, so only orders of magnitude can be compared. Second, there is an important difference between polymer and lipid membranes. Polymer membranes are relatively thick, and therefore the influence of boundary effects is negligible. Moreover, the interior is homogeneous on the length scale of diffusion. This is certainly not true for lipid membranes. The width of the interface as determined by neutron diffraction experiments[25] turns out to be quite substantial, i.e., about 40% of the total membrane phase. X-ray measurements[26] indicate that the membrane interior is far from homogeneous. This is confirmed by recent molecular dynamics simulations of various lipid membrane systems.[8,27–30] Third, analyses of various permeation data clearly indicate a more complicated permeation process. As pointed out by Lieb and Stein,[31,32] the size dependency of the permeation of small molecules resembles the size dependency in soft polymers and not in liquid alkanes. Walter and Gutknecht[33] reached the same conclusion based on an even larger series of permeation data for polar as well as nonpolar penetrants.

Therefore, it is highly questionable whether a homogeneous solubility–diffusion mechanism gives an adequate description of the permeation process of small molecules. In order to account for the observed discrepancies, several modifications of this model are proposed, which can be classified into two categories: models that assume a special type of diffusion and models that assume the presence of structural defects.

B. Special Diffusion. Walter and Gutknecht[33] showed that the solubility data alone could not explain the size effect on observed permeation rates. Therefore, they concluded that it should be the diffusion part of the permeation process which accounts for the observed relatively high permeability rates of smaller molecules. Instead of a diffusion process resembling diffusion in bulk alkanes, it resembles diffusion in soft polymer membranes.

Various diffusion theories[34,35] of soft polymers relate the diffusion rates of penetrant molecules to the available free volume of the membrane. They assume a hopping type of diffusion, which means that the penetrant makes a diffusive step when it is able to move suddenly from one free volume pocket to the next. The rate of diffusion depends on the distribution of the free volume pockets as well as on the movement of the polymer matrix. This is in agreement with the experimental picture. Quantitative predictions from the free volume theories are difficult, however. Either the assumptions are too crude or the theory becomes too specific. A straightforward transfer to lipid membranes seems therefore difficult.

Lieb and Stein[31] used the free volume theory of Cohen and Turnbull[36] to account for the temperature effect on permeation rates across lipid membranes. However, this theory was originally derived for atomic liquids and predicts an exponential size dependency of the free volume distribution whereas power laws are observed in polymer systems, both by experiment[37] and by computer simulations.[38,39] A recent renormalization theory of Nonnenmacher[40] assumes a cooperativity between polymer chains to be the cause for the deviation from exponential behavior. Percolation theory[41] also predicts power law behavior near the percolation threshold of the free volume in various kinds of systems. Whether this is the case in lipid membranes as well remains an unsolved question.

A free volume related type of diffusion was predicted by Traüble[23] ("mobile kink"), who assumed that the fast diffusion of small molecules is made possible by the presence of small free volume pockets which diffuse rapidly taking the penetrant along. His model successfully predicted the high permeation rate of a small penetrant but did not account for the permeation rates of larger penetrants. Besides, he assumed a highly ordered membrane which is more representative for the gel state.

The importance of free volume for the diffusion process is apparent from the observation by Potts and Francoeur[3] of a direct relation between diffusion rate and number of gauche angles in the lipid tails. The presence of gauche angles disturbs an efficient alignment of the tails and thus increases the amount of free volume.

An inhomogeneous diffusion process was concluded from permeability experiments on endothelial cells.[20] It appeared that the membrane consists of two distinct regions: the lipid headgroup

area behaving like a non-Stokesian medium and the membrane interior resembling a Stokesian fluid. A similar description of the membrane is given by Fettiplace and Haydon,[42] i.e., assuming two distinct regions with different diffusional resistances.

C. Defects. The model of Deamer and Bramhall[43] also adds an inhomogeneous aspect to the solubility–diffusion mechanism. They assume the presence of strands of water molecules extending into transient defects in the interface, with individual molecules breaking away from the edge of the strands. The length of the strand is assumed to be only a few water molecules, stabilized both by hydrogen bonds and by the ordering effect of the parallel hydrocarbon chains surrounding them.

The occurrence of even more extensive (but rare) defects, such as the transient formation of a pore allowing many water molecules and other penetrants to pass the membrane at once, has also been mentioned as contributing to the permeation process.[44] This possibility, however, predicts permeation rates that depend too little on the hydrophobicity of the penetrant molecule.[32] Moreover, Levitt[45] showed that the ratio between permeability for diffusional exchange of water and for net movement as in osmosis has to be equal to the number of water molecules present in the pore. Since the experimentally determined ratio is close to one, the presence of pores that allow simultaneous passage of a number of water molecules seems not to be a significant pathway for permeation of uncharged penetrants.

3. Theory: Inhomogeneous Solubility–Diffusion Mechanism

Considering the limiting predictive power of the homogeneous solubility–diffusion model and its apparent oversimplification of the lipid membrane, we now derive an inhomogeneous solubility–diffusion model. In this model, which is applicable to permeation of small molecules in general, the diffusional theory of transport is described in terms of the thermodynamics of irreversible processes. This enables us to link the permeation coefficient to experiments (subsection B) as well as to an integral over local properties in the inhomogeneous membrane (subsection A), which can be computed from the MD simulations (section 4).

A. General Diffusion Theory of Transport. We consider the motion of particles of the ith species (in this case water, but the theory is applicable to any solute as well) in the diffusional limit, where the average velocity, $u_i = \langle v_i \rangle$ is proportional to the thermodynamic driving force, which is the negative gradient of the thermodynamic potential μ_i:

$$u_i = -\frac{1}{\xi_i}\nabla\mu_i \tag{1}$$

where ξ_i is the frictional coefficient of the particles. (Note that if the thermodynamic potential is expressed in J/mol, the frictional coefficient is expressed per mole of particles as well.) The flux J_i in mol m^{-2} s^{-1} is given by

$$J_i = c_i u_i = -\frac{c_i}{\xi_i}\nabla\mu_i \tag{2}$$

The friction coefficient ξ_i is related to the diffusion constant D_i via Einstein's relation

$$D_i = RT/\xi_i \tag{3}$$

as can be easily seen when a concentration gradient in an ideal solution is considered for which $\mu_i = \mu_i^0 + RT \ln c_i$, and eq 2 reduces to Fick's law:

$$J_i = -D_i\nabla c_i \tag{4}$$

The linear flux relations for the case that material properties depend on one coordinate z can be written as

$$J_i(z) = -\frac{c_i(z)\, D_i(z)}{RT}\frac{\mathrm{d}\mu_i(z)}{\mathrm{d}z} \tag{5}$$

This is a one-dimensional Onsager relation, relating a flux to a driving force. For the case of more than one component there will in general be cross terms between the fluxes and driving forces. We shall, however, restrict our consideration to cases where the molecules diffuse independently through the membrane, experiencing only friction with the fixed membrane components. Then no cross terms arise. Together with the conservation law

$$\frac{\mathrm{d}J_i(z)}{\mathrm{d}z} + \frac{\mathrm{d}c_i(z)}{\mathrm{d}t} = 0 \tag{6}$$

eq 5 predicts the spatial and temporal evolution of the local density distribution. We are, however, interested in the steady-state solution of the flux in the linear regime, i.e., under the influence of a small deviation from equilibrium. Steady state means that J_i is not a function of z, and after rearranging we can integrate eq 5 over the membrane from z_1 in the bulk phase on one side to z_2 in the bulk phase of the other side:

$$\Delta\mu_i = \mu_i(z_2) - \mu_i(z_1) = -J_i RT \int_{z_1}^{z_2} \frac{\mathrm{d}z}{c_i(z)\, D_i(z)} \tag{7}$$

Here $c_i(z)$ is the concentration of component i in the presence of the imposed gradient. Under the assumption of small gradients, we can replace this concentration by the equilibrium concentration $c_i^{eq}(z)$ in the absence of an imposed gradient. If we define the permeation resistance R_i^P as

$$R_i^P = c_i^* \int_{z_1}^{z_2} \frac{\mathrm{d}z}{c_i^{eq}(z)\, D_i(z)} \tag{8}$$

where c_i^* is the concentration in the bulk solutions on either side of the membrane in the absence of an imposed gradient, the linear response relation, eq 7, becomes

$$J_i = -\frac{c_i^* \Delta\mu_i}{R_i^P RT} \tag{9}$$

The permeation resistance is directly related to the experimental permeability coefficient (next subsection) and is also amenable to computation on the basis of detailed simulation (section 4).

The assumptions that have been made so far, either explicitly or implicitly, in the derivations are the following: (1) The whole system is isothermal at absolute temperature T. (2) The membrane component is stationary in the frame of reference. (3) The local diffusion model is valid; i.e., the thermodynamic gradient can be considered constant over the correlation distance of the particle. (The distance given by the displacement of a particle during the time over which its velocity correlation function differs from zero.) (4) The fluxes are proportional to the gradients in the thermodynamic potential. This means that the limit of small gradients is considered where this is needed. (5) The permeation process is dominated by single molecules that only feel friction with the stationary membrane component.

Assumption 3 is the most questionable one, because the concentration gradients in a membrane are very large and the diffusion is relatively fast. It is possible to refine the barrier-crossing dynamics by including details of the velocity (or force) autocorrelation of the particles,[46] but we restrict our considerations to the simple diffusional limit.

Within the homogeneous solubility–diffusion model, the approximations are much more drastic. In addition to the assumptions mentioned above, it is assumed that (1) the membrane/water system exists as a two-phase system with a sharp boundary between the water and membrane phase, (2)

both phases are isotropic and homogeneous, and (3) the membrane phase has a well-defined width.

Using these assumptions, the equilibrium concentration c_i^{eq} and the diffusion constant D_i become independent of the position z in the membrane, and the permeation resistance (eq 8)simplifies to

$$R_i^p = d/S_iD_i \tag{10}$$

Here $S_i = c_i^{eq}/C_i^*$ is the solubility coefficient of the ith component in the lipid phase, and $d = z_2 - z_1$ is the thickness of the membrane.

B. Experimental Quantities. The driving force for permeation processes can be imposed by the following causes: hydrostatic pressure difference Δp (water), osmotic pressure difference $\Delta\Pi$ (water), or concentration difference Δc (solute or water isotope). Hydrostatic and osmotic differences are equivalent in their influence on the thermodynamic potential of water:

$$\Delta\mu_w = (\Delta p - \Delta\Pi)/c_w^* \tag{11}$$

Comparing eq 9 with eq 11, the flux can be expressed as

$$J_w = -\frac{1}{R_w^p}\frac{\Delta p - \Delta\Pi}{RT} \tag{12}$$

For the flux J_{is} of an isotope of water, we consider the z-dependent mole fraction $x_{is}(z)$ of the isotope. Its thermodynamic potential is given by

$$\mu_{is}(z) = \mu_w(z) + RT \ln x_{is}(z) \tag{13}$$

Assuming water to be in equilibrium over the membrane, μ_w is constant and equal to its bulk value μ_w^*. Integration of eq 5 using eq 13 and equating $c_{is}(z)$ with $x_{is}(z)\, c_w(z)$, we find

$$J_{is} = -\frac{1}{R_w^p}\Delta c_{is} \tag{14}$$

where $\Delta c_{is} = c_w^*\Delta x_{is}$ is the concentration difference of the isotope across the membrane. For the flux of a solute resulting from a (small) concentration difference Δc_s over the membrane, for which

$$\Delta\mu_s = RT(\Delta c_s/c_s^*) \tag{15}$$

it is easily derived that

$$J_s = -\frac{1}{R_s^p}\Delta c_s \tag{16}$$

The permeability coefficient P_i is usually defined as the ratio between flux and concentration difference, and thus P_i is equivalent to the inverse of the permeation resistance R_i^p defined by eq 8:

$$R_i^p = 1/P_i \tag{17}$$

4. Method of Simulation

This section describes how the permeability coefficient of water through a lipid membrane can be computed and how the molecular mechanism underlying the permeation process can be understood from MD simulations. Subsection A describes the parameters used for the actual MD simulation of the membrane. The method of computation of the permeability coefficient is given in subsections B–D. The last two subsections, E and F, deal with the analysis of free volume distribution in the membrane and the computation of radial distribution functions in an inhomogeneous system, respectively.

A. Simulation Parameters. The simulation box contains 64 dipalmitoylphosphatidylcholine (DPPC) molecules arranged in a bilayer, together with 736 water molecules. An equilibrated system was obtained by using the last time frame (160 ps) of the previous runs on this system.[7,8] The system is subject to periodic boundary conditions (so actually a multilamellar system is simulated). The system is coupled to a temperature bath at 350 K and a constant-pressure bath of 1 atm with coupling time constants of 0.1 and 0.5 ps.[47] The box lengths are scaled independently. The time step for integration of Newton's equations of motion is set to 2 fs. Short-range forces are cut off at a distance of 0.85 nm. The long-range electrical forces are calculated using a cylindrical cutoff of 1.8 nm in the lateral direction and no cutoff in the direction perpendicular to the membrane.

We applied the GROMOS[48] force field, with some modifications needed to bring the system into the (biologically relevant) liquid-crystalline phase. Atomic detail is used except for methyl groups which are treated as united atoms. The water is modeled as SPC.[49] More details about the simulation method plus a complete description of the force field can be found in the previous publications.[7,8] The only difference in the force field between the previous simulations and the ones presented here is the enlargement of the repulsive Lennard-Jones (LJ) parameters between methyl and polar oxygen atoms (including SPC oxygen). An MD study of the interface between decane and SPC water revealed that the solubilities of decane in water and vice versa were too high in the previously used force field.[50] Various LJ parameters were tested for this system, and a few new sets were modeled which predicted much better solubilities. The set of parameters of model C ($\sigma_{CH_3-O} = 0.310$, $\epsilon_{CH_3-O} = 0.637$, $\sigma_{CH_2-O} = 0.310$, $\epsilon_{CH_2-O} = 0.529$) turned out to be well behaved in constant-pressure simulations. The change of parameters in comparison with our previous simulation did not seem to have a significant effect on the structural properties of the membrane, however. The calculated free energy data on the other hand showed a small but significant dependence upon changing the parameters.

In order to calculate the position-dependent free energy and diffusion profiles, we performed three simulations with constrained water molecules of 120 ps each. Additional simulations of totally 150 ps were performed to study the movement of unconstrained water molecules. The simulations were carried out on a Cray-YMP supercomputer, with a speed of 5 ps/h CPU time.

B. Computation of the Permeability Coefficient. We now consider how the local equilibrium water concentration, expressed as a ratio to the bulk concentration, $c_w^{eq}(z)/c_w^*$, as it figures in the integrand of eq 8, can be computed from simulations. The local equilibrium water concentration is proportional to the probability that the system resides in phase space with the restriction that the z coordinate of one particular water molecule (z_0) occurs in the interval (z,z+dz). The local concentration is therefore proportional to the constrained partition function Q':

$$c_w^{eq}(z) \sim Q'(z) = a\int \mathrm{d}r_1 \ldots \mathrm{d}r_N\, \delta(z_0 - z)\, \exp\{-V(r_1 \ldots r_N)/kT\} \tag{18}$$

where a is a constant. The ratio $c_w^{eq}(z)/c_w^*$ is given by the ratio of $Q'(z)$ and $Q'(z_1)$ at position z_1 in the bulk solution. This ratio can be related to the potential of mean force ΔG relative to the bulk phase:

$$\Delta G_w(z) = -RT \ln\frac{Q'(z)}{Q'(z_1)} = -RT \ln\frac{c_w^{eq}(z)}{c_w^*} \tag{19}$$

Thus, the permeation resistance, eq 8, can also be expressed in the potential of mean force

$$R_w^p = \int_{z_1}^{z_2}\frac{\exp(\Delta G_w(z)/RT)}{D_w(z)}\,\mathrm{d}z \tag{20}$$

The challenge now is to obtain the potential of mean force as well

as the local diffusion constant of water in the membrane. Once this is computed, the integration can be performed numerically, and the permeability coefficient can be obtained from eq 17.

C. Computation of the Potential of Mean Force. In practice, the potential of mean force can be computed from simulations using different methods, each method having its limited range of accuracy. We used three different methods (described below) in three distinct regions of the membrane.

Analysis of Local Density. This method directly evaluates the local equilibrium concentration of water across the membrane, and $\Delta G(z)$ follows immediately from eq 19. The membrane is sectioned into slices, and the number of water molecules is counted per slice and averaged over the length of the simulation. The statistics of particle counting can be assumed to follow a Poisson distribution. If the average number of particles in a slice equals N per configuration and n statistically independent configurations are generated, the relative error in ΔG equals $RT/(Nn)^{1/2}$. The error becomes large at low concentrations. Since the penetration of water into the bilayer is a rare process on a molecular dynamics time scale, no reliable information can be obtained for the local equilibrium concentration of water in the membrane interior. Using the experimentally determined permeation rates of around 10^{-2} cm/s (converted to 350 K, the simulation temperature), one would expect at most one water molecule to permeate the bilayer during the total simulation time.

Particle Insertion. A very elegant method is the particle insertion method of Widom.[51] The procedure is to insert a water molecule as a "ghost" particle, i.e., without disturbing the configuration, randomly into the region of interest and determine its interaction energy E_{ins} with the "real" particles. Now define its Boltzmann factor, averaged over many insertions, as the insertion thermodynamic potential μ^{ins}:

$$\Delta\mu^{ins}(z) = -RT \ln \langle \exp(-E^{ins}(z)/kT) \rangle \qquad (21)$$

In the case of a very dilute solution $\Delta\mu^{ins}$ measures the difference in standard thermodynamic potential of the solution (water in the membrane phase) and the ideal gas, referred to the same standard concentration:

$$\mu^0{}_{solution}(z) = \mu^0{}_{ideal\ gas} + \Delta\mu^{ins}(z) \qquad (22)$$

In the interior of the membrane, water is so dilute that it forms an ideal solution with concentration $c^{eq}(z)$, which is in equilibrium with bulk water outside the membrane, with thermodynamic potential μ^*:

$$\mu^* = \mu^0{}_{solution}(z) + RT \ln c^{eq}(z) \qquad (23)$$

From eqs 19, 22, and 23 it follows that

$$\Delta G(z) = \Delta\mu^{ins}(z) + [\mu^0{}_{ideal\ gas} + RT \ln c^* - \mu^*] \qquad (24)$$

Equation 24 shows that the potential of mean force can be "measured" by the insertion thermodynamic potential but shifted by a correction term, given between the brackets. The correction term is constant at a given temperature and was found to be +26.8 kJ/mol at 300 K for the water model used (SPC) by thermodynamic integration.[52] The temperature-dependent data for the SPC model show that the entropy remains fairly constant over the temperature range 273–373 K, which enables us to estimate the correction term to be +24.3 kJ/mol at 350 K. These values are very close to the experimental values for bulk water, which are equal to

$$[\ldots] = RT \ln(RTc^*/p_{sat}) \qquad (25)$$

assuming ideality of the saturated vapor. Here p_{sat} is the saturated vapor pressure. At T = 300 K (density 996.57 kg/m^3, p_{sat} = 3567 Pa) the correction term is 26.35 kJ/mol, and for T = 350 K (density 973.61 kg/m^3, p_{sat} = 41 905 Pa) it is 23.95 kJ/mol.

The major problem with the particle insertion method is that it only works well if the number of successful insertions (i.e., insertions with low energies) is large enough to sample the phase space sufficiently. The fulfillment of this criterium can be checked by computing the distribution of states, $f(E^{ins})\,dE$, which is the product of the probability $p(E^{ins})\,dE$ finding an interaction energy in the interval $(E^{ins},E^{ins}+dE)$ and its Boltzmann factor:[53]

$$f(E^{ins})\,dE = \exp(-E^{ins}/kT)\,p(E^{ins})\,dE \qquad (26)$$

The phase space is sampled sufficiently if the distribution of states is sampled well across its maximum value. As long as this is not the case, the computed thermodynamic potential will be an overestimation of the real value. When the sampling is done sufficiently, the error in the average Boltzmann factor (and thus in the insertion thermodynamic potential) can be estimated from performing the averaging of the Boltzmann factors in a number of blocks separately and compute the standard deviation. The error becomes large if the density of the system increases (and therefore the number of successful insertion drops) and normally cannot be applied for fluidlike systems. Only in the middle part of the membrane, where the density is quite low, could this method be applied. In order to obtain random insertions, the ghost particles were placed on a homogeneous grid, mapped onto the system. Random rotations were computed using a quarternion formalism.[54]

Applying the particle insertion method, it is in principle possible to compute at the same time, apart from the chemical potential, also the molar enthalpy h^{ins}:

$$\Delta h^{ins}(z) = \frac{\langle E^{ins}(z) \exp(-E^{ins}(z)/kT) \rangle}{\langle \exp(-E^{ins}(z)/kT) \rangle} + \frac{\langle E^{ens} \exp(-E^{ins}(z)/kT) \rangle}{\langle \exp(-E^{ins}(z)/kT) \rangle} - \langle E^{ens} \rangle \qquad (27)$$

where E^{ens} is the interaction energy of the total ensemble in which the insertion takes place. However, the second and third term in eq 27 are large (as they apply to the energy of the complete ensemble). Therefore, the difference between these two terms will be very noisy and will only cancel if the energy of the inserted particle is uncorrelated to the energy of the ensemble. This will generally be not the case, especially in dense systems. Therefore, we restricted our computations to the first term of eq 27 and use this as a qualitative estimation of the enthalpy only. The molar entropy s^{ins} (with the same restrictions) can be obtained from

$$T\Delta s^{ins}(z) = \Delta h^{ins}(z) - \Delta\mu^{ins}(z) \qquad (28)$$

Average Force on Constrained Particle. It is possible to directly determine the derivative of the potential of mean force by measuring the average force exerted on a water molecule that is constrained at a given depth z in the membrane. This follows by taking the derivative of ΔG (eq 19):

$$\frac{d\Delta G(z)}{dz} = -\frac{RT}{Q'(z)}\frac{dQ'(z)}{dz} \qquad (29)$$

The derivative of Q' is found by partial integration of eq 18 to be

$$\frac{dQ'(z)}{dz} = -\frac{a}{kT}\int dr_1 \ldots dr_N\, \delta(z_0 - z)\frac{\partial V}{\partial z_0}\exp(-V/kT) \qquad (30)$$

Hence

$$\frac{d\Delta G(z)}{dz} = -N_{Av}\left\langle \frac{\partial V(r_1 \ldots r_N)}{\partial z_0} \right\rangle = -N_{Av}\langle F_z(z_0) \rangle \qquad (31)$$

where $\langle F_z(z_0)\rangle$ is the mean force on the constraint (i.e., the component of the force on the water molecule in the direction of the constraint z, averaged over the constant ensemble). This force is easily monitored during a constrained simulation: The constraint is imposed by resetting the z coordinate of the center of mass of an inserted water molecule each step to its original, constrained value z_0 (with respect to the center of mass of the system); the force is directly proportional to the distance over which the z coordinate is reset. No restrictions need to be applied in the xy direction, which means that the inserted particles are free to diffuse in the plane perpendicular to the bilayer normal and also free to rotate in all three directions around their center of mass. Repeating the constraining procedure for water molecules at different positions, the potential of mean force can be reconstructed upon integration of eq 31. The force fluctuates heavily, but a long simulation ($\sim$100 ps) nevertheless provides accurate averages. The accuracy can be estimated from the separate averaging over blocks of 10 ps. The average force method is especially useful in the part of the membrane just behind the interface, where the local equilibrium concentration of water is too low to use eq 19 and the lipid density too high to use eq 21.

Other Methods. Apart from the methods mentioned above, several other methods could be used alternatively. For example, one method is umbrella sampling, which restricts the sampling of phase space to a narrow region in the membrane by applying an additional potential for which a correction is made afterward. The method of computing the average force on a constrained particle can be considered as a limiting case of the umbrella sampling method, i.e., with an infinitely narrow restricting potential. The advantage of the average force method is that it allows for the computation of the local diffusion constant at the same time (see subsection D).

Another method that could be used is the determination by thermodynamic integration of the free energy needed to materialize a particle at a given point in space. This method, however, involves additional inaccuracies and has no advantages above the methods we used.

D. Computation of Local Diffusion Constants. As is the case for the computation of the local potential of mean force, there exist different methods to compute local diffusion constants or, similarly, local friction coefficients. We applied two different methods.

Mean-Square Displacement. The easiest way to calculate the diffusion coefficient in an MD simulation is from the mean-square displacement (MSD) of the water molecules. The slope of the MSD curve is proportional to the diffusion coefficient. For diffusion in the z direction we have

$$D(z) = \lim_{t\to\infty} \langle (z(t) - z(0))^2\rangle/2t \tag{32}$$

The time origin ($t = 0$) can be shifted to improve statistics. In the interfacial region there are enough water molecules to obtain a reasonably accurate value for the diffusion coefficient using this method. The diffusing process itself, however, makes it difficult to calculate the diffusion constant locally in the membrane. During the observation of its displacement the particle wanders through regions with different diffusion constants. If only those particles are selected that remain in a given region during a sufficiently long time, an unacceptable bias is introduced. The best way of computing the local diffusion constants turned out to be by the consideration of diffusion within short time intervals (1–5 ps) only. The geometric center of the considered short-time diffusion trajectory determines its approximate position in the membrane. The use of different time intervals offers an estimate of the bias introduced. Although the permeability coefficient only depends on the diffusion rate perpendicular to the membrane (z direction), the lateral diffusion constant (xy plane) can also be computed using the MSD method for comparison. Naturally, the membrane interior which is devoid of water molecules demands another approach.

Force Autocorrelation Method. A general method that can be used to study diffusion over free energy barriers[55] is based on the fluctuation–dissipation theorem.[56] Via this theorem the autocorrelation function of the random forces $\Delta F(t)$ acting on a molecule is related to the local time-dependent friction coefficient $\xi(z,t)$:

$$\xi(z,t) = \langle \Delta F(z,t)\, \Delta F(z,0)\rangle/RT \tag{33}$$

Time integration of this equation gives the local static friction coefficient ξ^s. Assuming that during the decay time of the time-dependent friction coefficient the particles remain in a region of constant free energy, the static friction coefficient can be related to the local diffusion coefficient via Einstein's relation:

$$D(z) = RT/\xi^s(z) = (RT)^2/\int_0^\infty \langle \Delta F(z,t)\, \Delta F(z,0)\rangle\, \mathrm{d}t \tag{34}$$

The required local random forces can be obtained from the forces on the position-restrained water molecules (needed for the calculation of the potential of mean force, see previous section). The deviation of the instantaneous force from the average force acting on these molecules is the required random force:

$$\Delta F(z,t) = F(z,t) - \langle F(z,t)\rangle \tag{35}$$

Other Methods. Instead of relating the friction coefficient to the force fluctuations (eq 34), one can also compute the friction coefficient from the response to an externally applied force F^{ext}:

$$\xi(z) = F^{ext}(z)/\langle v(z)\rangle \tag{36}$$

where $\langle v(z)\rangle$ is the average velocity of the particle to which the external force applies. This method has been applied successfully to obtain diffusion rates from MD simulations.[5,57] We chose the force autocorrelation method since it allows the computation of the free energy profile at the same time (see subsection C).

E. Computation of Free Volume. According to free volume theories, the distribution of free volume in the membrane is directly related to the diffusion rate of permeant molecules in the membrane. It will also (partly) relate to the chemical potential of water molecules in the membrane. The percentage of free volume can be computed locally in the membrane using a uniform grid. Two kinds of free volume are distinguished. The first, which we will call "empty free volume", conforms to the definition given by Bondi[58] and is computed as the percentage of grid points lying outside the van der Waals radii σ_i of any of the system atoms. The second one, the "accessible free volume", is calculated in the same way except for the addition of the van der Waals radius of the penetrant molecule, σ_j, to the radii of the system atoms. In the limiting case of a penetrant with zero radius, empty free volume and accessible free volume are equal.

F. Computation of Pair Distribution Functions. The radial pair distribution functions (RDF's) of water and lipid atoms will give information about the amount of bound and unbound water in the different regions of the membrane. This will in turn connect to the observed diffusion rates. In an inhomogeneous system, the pair radial distribution function $g(r)$ between (specific) headgroup atoms i and water molecules w is computed from

$$g(r) = \frac{1}{N}\sum_{i=1}^{N_i}\sum_{w=1}^{N_w} \frac{\delta(r - r_{iw})}{\rho_w(z_i,r_{iw})4\pi r^2} \tag{37}$$

where N_i is the number of headgroup atoms and $\rho_w(z_i,r_{iw})$ is the local water density at a distance r_{iw} between water molecule w and headgroup atom i, which resides at position z_i along the membrane. In homogeneous systems, this water density factor is simply constant and can be replaced by ρ_w, the average water density. Across the membrane, however, the water density as seen by the headgroup atoms is far from homogeneous, and computing of the uncorrected RDF leads to hydration peaks which

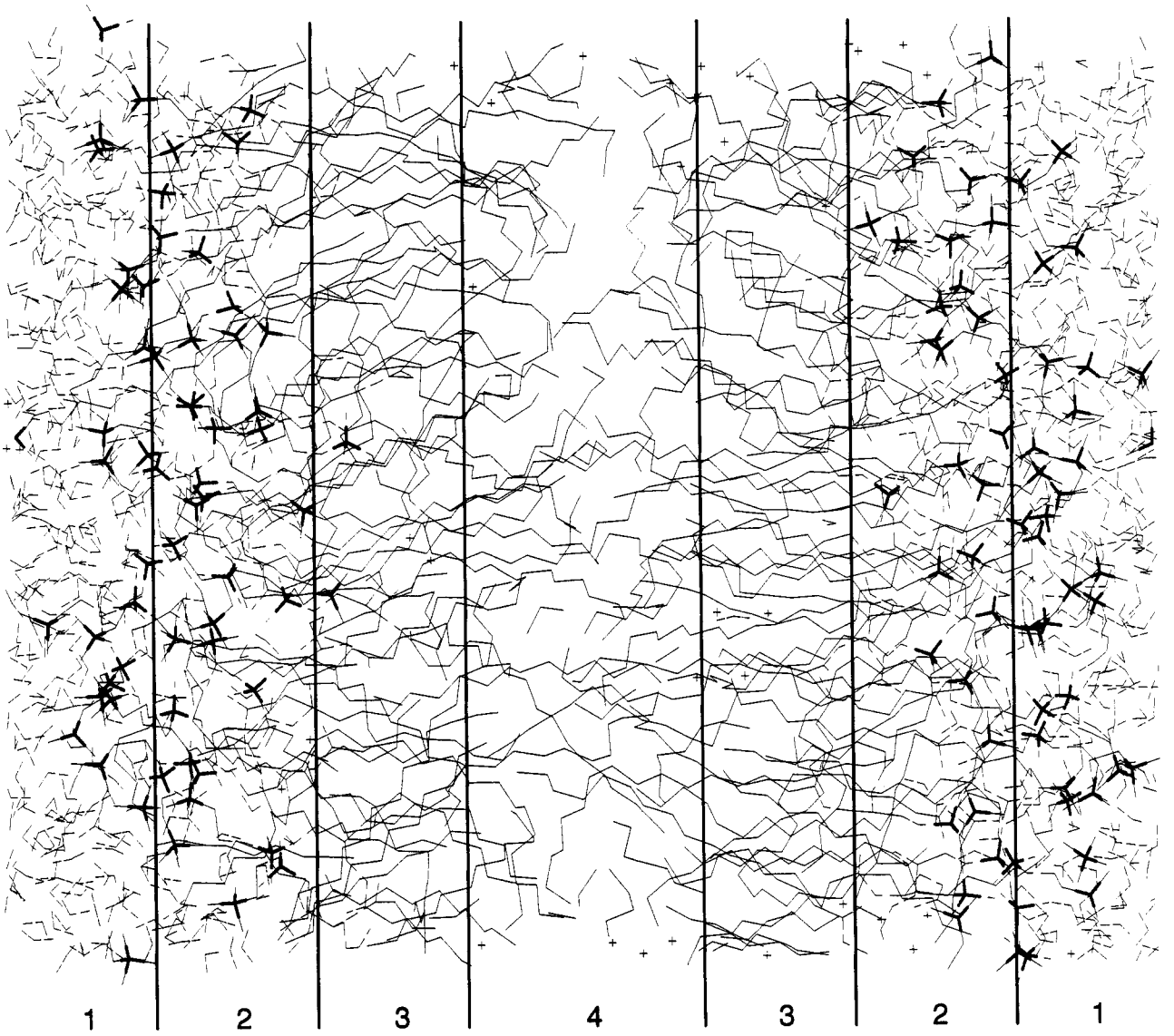

Figure 1. Snapshot of simulated membrane. Dashed lines are used for water molecules and bold lines for choline and phosphate groups. Vertical lines indicate the boundaries between the different regions (see text for definitions). Crosses result from bonds cut by the boundary planes.

reflect primary the bulk water density as seen from the average position of the specific headgroup atoms. In order to calculate the local water density factor, a uniform grid was mapped onto the system, and for every grid point the radial density function of water molecules was calculated. Averaging over an xy plane of grid points resulted in radial water density functions for various positions z along the bilayer normal. The position along the z axis of a specific headgroup atom determines the choice of the density function used to scale its pair distribution function (eq 37). In this way, the total density of water molecules seen by the headgroup atoms is scaled to the bulk water density. It is therefore possible to compare the different pair distribution functions irrespective of the average position of the considered molecules in the system. To obtain actual hydration numbers, however, the density *uncorrected* RDF's should be used. Hydration numbers are obtained by integrating the RDF's to the first minimum.

5. Results

A. Proposal of the "Four-Region" Model. Our previous simulations[7,8] already revealed that the water/phospholipid bilayer system differs considerably from a two-phase alkane/water system. This is confirmed by other MD simulations of phospholipid membranes[27-30] as well as by experimental measurements.[25,26] Instead of a sharp interface, a very diffuse interface between the dipolar headgroups and water is observed. Besides, the hydrocarbon interior of the membrane shows a very inhomogeneous character, unlike bulk liquid alkane. Also, the dynamical behavior of the lipids is highly anisotropic, which can be very clearly seen on a video movie of the system.[59] A two-phase model seems therefore not suitable to describe the permeation process, and therefore we decided that it would be better to look at the permeation process within the framework of a more sophisticated model, which takes into account the inhomogeneity of the whole membrane. This model splits the membrane up into four regions, each of which has its own special characteristics. The first two regions belong to the interface of the membrane; the other two regions describe the interior of the membrane. Based on all analyses that have been done on the system, the definition of the four regions is as follows. (See Figure 1 for a graphical representation and the exact location of the regions.)

Region 1: *Low Headgroup Density*. This region starts at the point where the presence of the membrane begins to result in a perturbation of the bulk water structure until the water density and the headgroup density are comparable. This region can actually be very large since the perturbation of water molecules can in principle extend over a long distance.

Region 2: *High Headgroup Density*. The water density drops to less than 1%. Total width of this region is 0.75 nm. In this region bulklike water is no longer present.

Region 3: *High Tail Density*. This region starts at the edges of the penetrating strands of water until the density of the

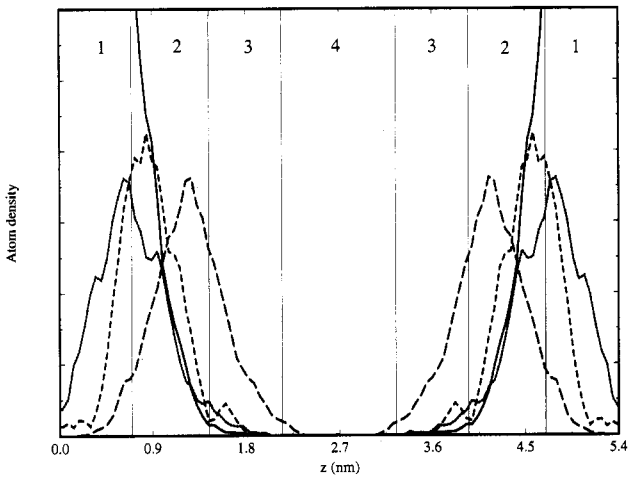

Figure 2. Distribution of interfacial atoms. Solid, dotted, dashed, and long dashed lines are used for water (H_2O), nitrogen (N), phosphorus (P), and carbonyl groups (C=O), respectively. The middle of the water layer corresponds to $z = 0.0$ and $z = 5.4$. Vertical lines indicate the different regions.

membrane has dropped to that of liquid hexadecane and measures 0.7 nm. The density of the membrane in this region is high.

Region 4: Low Tail Density. The remaining (=middle) part of the membrane represents the fourth region. The width is 1.1 nm (both halves of the bilayer). In this region the lipid density is much lower than in region 3, comparable to liquid hexane.

In all subsequent figures the position of the regions, as defined above, will be indicated. It should be stressed that the exact locations of the boundary regions are somewhat arbitrary and most certainly will differ in other membrane systems. However, the qualitative idea of the fourth-region model is considered to be applicable to other bilayer membranes as well.

In the next two subsections a detailed picture is presented of the structural and dynamical aspects of the four regions in the membrane that are important for understanding the results of the permeation process. Subsection B describes the interface (regions 1 and 2), and subsection C describes the membrane interior (regions 3 and 4). The other subsections (D to G) deal with the actual permeation process.

B. Description of the Membrane Interface. Examination of the lipid/water boundary reveals (see Figure 1) that no sharp interface has been formed. Groups of water molecules penetrate into the membrane, and some lipid headgroups protrude into the middle of the water layer. The distributions of water and headgroup atoms are plotted in Figure 2. The distributions show a large overlap, with still a considerable water concentration at the carbonyl groups at the beginning of the lipid tails but with a membrane interior without a detectable density of water molecules. Experimental data[26,60] confirm these findings. Defining the width of the interface as the distance required for the water concentration to drop from 90% to 1% (i.e., regions 1 and 2, leaving out the region of only slightly perturbed water), we find an interface width of 1.1 nm. Taking both interfaces into account this means that approximately 40% of the total membrane belongs to the interfacial part.

The structure of the interfacial water is clarified in terms of radial (pair) distribution functions (RDF's). Figure 3 shows the RDF's of water–water pairs at different positions in the interface. Two sets are shown: one set that is normalized to the average water density in the system and another which is corrected for the inhomogeneous water density (see section 4).

From the uncorrected RDF's we can obtain the average number of nearest neighbors. It drops from 4.8 (close to bulk SPC[47]) in region 1 down to 1.0 at the edge of regions 2 and 3. Almost no singly dispersed water molecules are observed. As can be seen clearly from the density corrected RDF's, the first hydration peak strongly depends on the position of the water molecule in

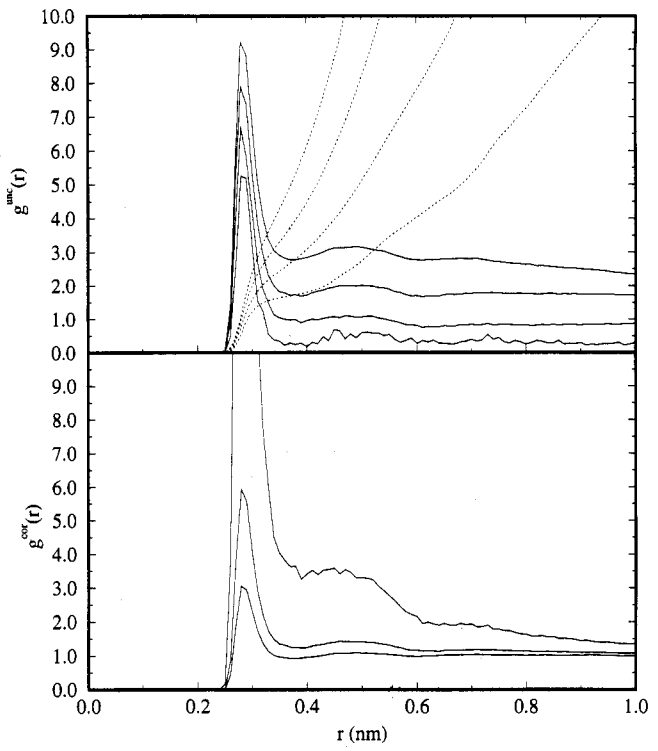

Figure 3. Radial distribution functions of water–water pairs. Uncorrected $g(r)$ (upper) as well as corrected $g_{corr}(r)$ (lower) for inhomogeneous water density. Different curves are computed in different regions. From bottom to top: region 1, boundary region 1/2, region 2, and boundary region 2/3 (uncorrected only). Dashed curves represent running coordination numbers.

the interface. This means that the effective hydration is much stronger in region 2 than in region 1. It seems that the water molecules form strands that penetrate into the membrane, thereby trying to keep at least one hydrogen bond to a neighboring water molecule. This observation is in good agreement with the analysis of hydrogen bond capacity in MD simulations of the same system used to study the ordering of water between membranes.[61] It was shown that as the water density drops, the ability of making hydrogen bonds to neighboring water molecules increases. Starting with a value close to the bulk SPC value (0.56), the fraction of nearest neighbors of a water molecule being hydrogen bonded to it attains finally, at the edge of regions 2 and 3, a value of 1.0. Since the number of nearest neighbors at this point also has dropped to 1.0, this means that water molecules in this region only have one more neighboring water molecule to which they are strongly hydrogen bonded.

From the radial distribution functions of headgroup–water pairs it is deduced that especially the choline–methyl, phosphate–oxygen, and carbonyl–oxygen groups are hydrated. Their RDF's are shown in Figure 4, corrected as well as uncorrected for the inhomogeneous water density. First hydration shells are clear; second hydration shells can also be detected (except for carbonyl). All headgroups show an increased hydration capability when they are buried deeper into the membrane. The diminished opportunity for water molecules to make water–water hydrogen bonds obviously results in an enhanced number of headgroup–water hydrogen bonds. Comparing the density-corrected RDF's of the different headgroups, it appears that the choline group is the most effective group for hydration in region 1, whereas the phosphate group is the most effective in region 2. This can be understood by comparing the partial charges on the atoms. The charge on the phosphate–oxygen is about twice as high as on the choline–methyl and carbonyl–oxygen, which in principle will result in a stronger (and larger) hydration shell. However, in the water layer the accessibility of the methyl groups is much larger. (They are at the end of the headgroup.) This effect apparently overcompensates for the smaller partial charges. The density-

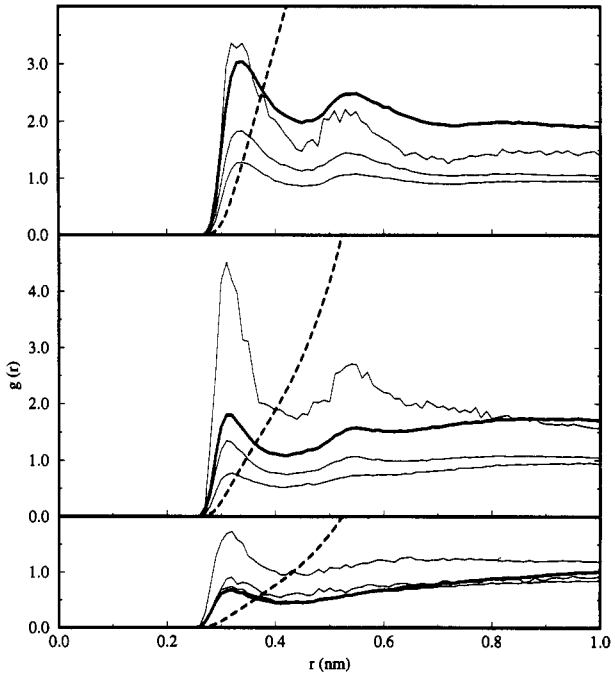

Figure 4. Radial distribution functions of headgroup–water pairs. Choline methyl (NCH_3, upper), phosphate oxygen (PO, middle), and carbonyl oxygen (C=O, lower) headgroup–water pairs are shown. Thick lines are used for the density-uncorrected RDF's, together with the running coordination numbers (dashed). Thin lines are used for the density-corrected RDF's, computed in different regions. From bottom to top: region 1, boundary region 1/2, and region 2.

uncorrected RDF's show that the choline–methyl groups have, on average, the largest hydration shell since it is on average mostly protruding into the water layer (see Figure 2). Integrating these RDF's to the first minimum, we find an average value of 12.5 choline-bound water molecules, i.e., about 4 waters per methyl group. The number of bound waters to a phosphate group as a whole is considerably less, 4.0 on average. A carbonyl group is only being hydrated on average by one water molecule. The low water density at the position of the carbonyl groups excludes larger hydration shells. Approximately 85% of the total number of water molecules take part in the hydration of headgroup atoms, implying that these water molecules are on average bound to 1.6 headgroup atoms. The total number of bound waters per lipid is therefore 11. Unbound water is only found in the middle part of the water layer. Computation of the autocorrelation functions for binding of the water to choline, phosphate, and carbonyl groups reveals that about 30% of the water molecules is strongly bound (with decay times of 50–100 ps), and the rest is predominantly weakly bound (decay times of 1–10 ps). In terms of number of water molecules this means that per lipid about three water molecules are strongly bound and the other eight weakly.

Experimentally, three types of water molecules are distinguished in lecithin membranes: water molecules in a hydration shell, either strongly or loosely bound, and interstitial water, trapped between the bilayers but not in a hydration shell. There is general agreement on the maximum water uptake, but it is not clear how many of the molecules are interstitial and how many are in a hydration shell. Also, the percentage of strongly and loosely bound water molecules is not clear. This is due partly to the difficulty of the measurements and partly to the vague definition of these three types of water. Therefore, the reported data are widely scattered. The number of bound water molecules per lipid falls usually in the range 9–14.[62-64] The only conclusion that can be drawn from the numbers of strongly and loosely bound waters seems to be that the larger part is loosely bound. Our numbers are in agreement with these findings.

C. Description of the Membrane Interior. Our MD simulations show that the membrane interior is far from homogeneous. In our previous work[7,8] we calculated the electron density profile,

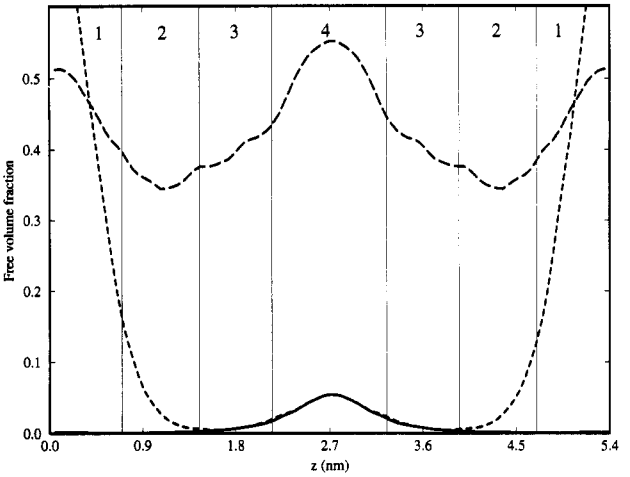

Figure 5. Free volume distribution. Curves represent empty free volume (long dashed) and water-accessible free volume including (solid) and excluding (dotted) the water molecules already present in the system. The middle of water layer corresponds to $z = 0.0$ and $z = 5.4$. Vertical lines indicate the different regions.

which conforms to the shape as determined by X-ray diffraction experiments.[12] The density is highest at the very beginning of the tails (1.10 g/cm^3) and lowest in the middle of the membrane (0.60 g/cm^3). For comparison, the density of liquid hexadecane is 0.73 g/cm^3 and of liquid hexane 0.61 g/cm^3 at $T = 350$ K (values derived from temperature-dependent measurements[58]). Higher densities are found in soft polymers (0.9–1.3 g/cm^3). In our previous work,[7,8] the tail order parameter profile was calculated to be in perfect agreement with experimental DMR data.[65,66] This profile shows that in the high-density region 3 the tails are more neatly aligned parallel to each other and therefore can pack in a more efficient way. Toward the middle of the bilayer (region 4) the number of gauche angles increases since they are more favored in the neighborhood of end groups. In addition, methyl groups pack with a lower density than methylene groups do.

For the permeation process of small molecules it is important to know the distribution of free volume in the membrane. We computed the empty free volume as well as the accessible free volume (for definitions, see section 4) for a water molecule. The result is plotted in Figure 5. As is to be expected, the shape of the free volume curve is similar to the shape of the electron density curve with the largest free volume found in the middle of the membrane. Experimentally, the empty free volume fraction in liquid hexadecane at 293 K is found to be 0.417.[58] At the boiling point (559 K) this value is 0.565. Using a linear interpolation, we estimated a value of 0.45 at the simulation temperature (350 K), which equals the calculated value of the membrane approximately halfway along the lipid tails, on the boundary between regions 3 and 4.

Looking at the water-accessible free volume (Figure 5), we see that only in the middle part of the membrane there is really free space available to accommodate a water molecule. The presence of free volume pockets in the high-density region is rare. Also, in the water layer itself very few free volume pockets exist, although the empty free volume fraction in water is comparable to that in the middle part of the membrane. This indicates that the free volume in the membrane has a different distribution function with relatively more large cavities. The subject of cavity distributions, connected to percolation theory, will be the topic of a forthcoming publication.

D. Analysis of the Free Energy Data. The calculated excess free energy profile is plotted in Figure 6. The profile is a reconstruction of three profiles that were obtained from applying three different methods (see section 4). In region 1 and partly region 2 most accurate values are obtained from the analysis of local density. In regions 2 and 3 the method based on the average force on constrained particles was used, and in the middle part

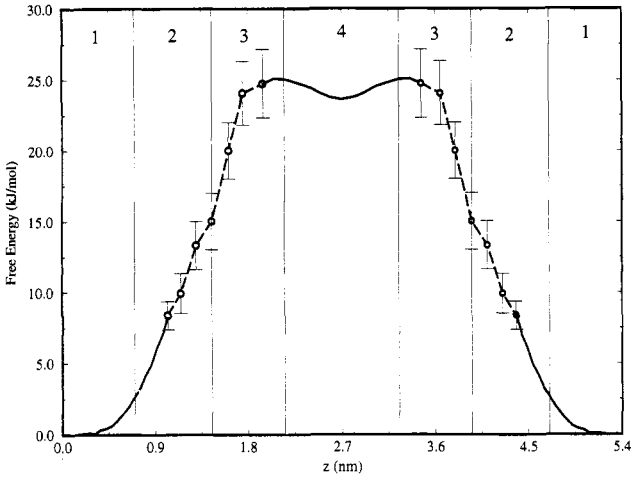

Figure 6. Excess free energy profile. The solid part in regions 1 and 2 was calculated from the local density of water molecules, the dashed part from the mean force on constrained water molecules, and the solid part in region 4 from the particle insertion method. The various curves are fitted together such as to obtain best possible overlap between the methods. The middle of the water layer corresponds to $z = 0.0$ and $z = 5.4$. Vertical lines indicate the different regions.

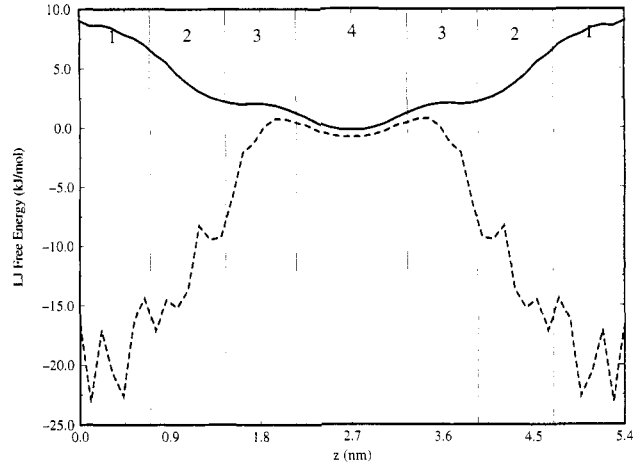

Figure 7. Free energy due to LJ interactions only, computed using the particle insertion method. Total free energy ΔG (dashed) and LJ free energy ΔG_{LJ} (solid) are shown. The middle of the water layer corresponds to $z = 0.0$ and $z = 5.4$. Vertical lines indicate the different regions.

of the membrane (region 4) the particle insertion method yielded the best results.

The shape of the free energy curve is approximately trapezoidal, in contrast to the step function assumed in the solubility–diffusion model. In region 1, the free energy is still close to the bulk value. A small increase is observed as soon as the lipid density increases because of the excluded volume. This increase gradually continues through regions 2 and 3 as the density increases and the possibility of making favorable hydrogen bonds to other water molecules and headgroup atoms diminishes. Also, the long-range electrostatic interactions become weaker. The maximum height of the free energy barrier is reached in region 4, close to the middle of the membrane. At this point the free energy barrier is 26 ± 2 kJ/mol. In the middle there is a small dip of about 1.5 kJ/mol. Although the water molecules in this part of the membrane are even further away from the (favorable) charges at the interface, the lower local density of tail groups results in a comparably more favorable environment. This behavior is also predicted by a mean field lattice theory.[67]

The value reported for the excess free energy of water in hexadecane is 25 kJ/mol.[1,68] This value compares well with the value we find at the border between regions 3 and 4 where the density is close to bulk hexadecane. Further evidence for the reliability of the computed free energies comes from the value of 25.2 ± 0.4 kJ/mol for the free energy of SPC in bulk decane, calculated by Widom's particle insertion method using the same simulation parameters.[50] The fact that the free energy value within the membrane is not significantly lower than in liquid alkanes indicates that (long-ranged) electrostatic field fluctuations are not important in the membrane interior. (The energy term is proportional to the square of the field.) With no charge density in the membrane interior, the symmetry of the membrane prohibits the presence of an average electrostatic field. The electrostatic potential that results from the charge distribution in the interface has been computed for this system and indeed decays very fast going into the membrane interior.[61] Approximately 1.0 nm away from the center of the interface (boundary between regions 1 and 2), the electrostatic potential has vanished. Therefore, a free energy value close to the value of bulk alkanes is to be expected in region 4.

In order to characterize the type of interaction that dominates the free energy, we applied Widom's particle insertion method with the Boltzmann factor based on the Lennard-Jones (LJ) energy only. Thus, we obtain the (unphysical) free energy for water in the absence of charges. The free energy due to LJ interactions only and the total free energy profile as determined by Widom's particle insertion method are plotted in Figure 7. Note that the profiles only predict quantitatively correct results in region 4, where the density in the membrane is low enough to allow a sufficient number of successful insertions. The other regions overestimate the real free energy. Qualitatively, however, it affirms our earlier conclusions, based on the accessible free volume distribution, that the most favorable LJ interactions are found in the middle of the membrane. In the denser regions LJ interactions become more repulsive. The favorable dipolar electrostatic interactions in the interface, however, result in the lower total free energy. Comparison of the free energy due to LJ interactions with the total free energy in region 4 shows that long-range electrostatic interactions are indeed unimportant in this region.

A further way of enhancing the understanding of the free energy profile is by computing the enthalpy and the entropy part. This information can also be obtained from the particle insertion computations, using eqs 27 and 28. Note, however, that we used the first term of eq 27 only. Besides, the same limitation holds as for the previous figure, i.e., that the computations only converged in the middle of the membrane. Therefore, the results should be interpreted in a qualitative way only, especially in the dense parts of the membrane. The enthalpy and entropy profiles are shown in Figure 8. Nevertheless, it is obvious from Figure 8 that the total enthalpy difference across the membrane is much larger than the free energy difference. The compensation comes form the entropy part, the shape of which looks similar to the shape of the free energy based on LJ interactions only (Figure 7). Likewise, the entropy profile can be understood considering the lower density toward the membrane interior, which allows more configurational freedom for the local water molecules and hence a more favorable entropy. The enthalpy is lowered toward the water layer by the presence of charges. The value of the enthalpy in the middle of the water layer is computed to be much lower than the enthalpy of −39.0 kJ/mol for bulk SPC at T = 349 K.[69] Highly probable, the neglected terms in eq 27 are significant in this region. In region 4 one sees that, although the free energy is comparable to that of the saturated vapor, the enthalpy contribution is still favorable (−5 kJ/mol), whereas the entropic contribution is slightly unfavorable (+5 kJ/mol).

E. Analysis of the Diffusion Data. The diffusion profile for the water molecules in the z direction is plotted in Figure 9. It is determined by combining the two methods described in section 4. In regions 1 and 2 the diffusion constants were calculated from the mean-square displacement and in regions 3 and 4 from the force correlation method.

In the middle of the water layer the headgroup density is low, and the water molecules diffuse almost as fast as in bulk SPC

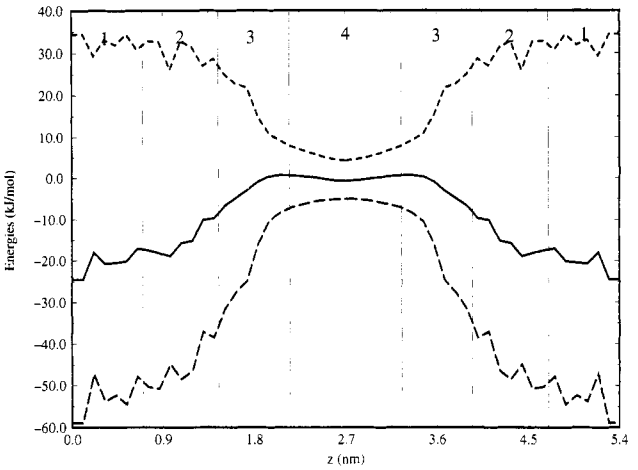

Figure 8. Enthalpy and entropy contributions to the free energy, computed using the particle insertion method. Free energy ΔG (solid), enthalpy ΔH (long dashed), and entropy $-T\Delta S$ (dashed) are shown. The middle of the water layer corresponds to $z = 0.0$ and $z = 5.4$. Vertical lines indicate the different regions.

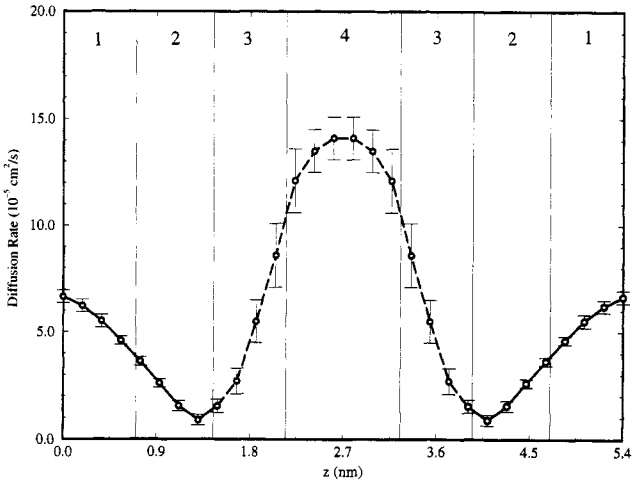

Figure 9. Diffusion rate profile. The solid part was calculated from the mean-square displacement and the dashed part from the force correlation method. The middle of the water layer corresponds to $z = 0$ and $z = 5.4$. Vertical lines indicate different regions.

water (7.5×10^{-5} cm^2/s at 350 K[47,69]). Note that the SPC model overestimates the diffusion rate of real water with a factor of ~ 1.3 at this temperature. Upon going toward region 2 more and more water molecules become bound to the lipid headgroups, and hence the diffusion rate decreases almost an order of magnitude. This value still is much larger than the self-diffusion rate of the lipids, which is of the order of 10^{-7}–10^{-8} cm^2/s.[70-73] Therefore, a large part of the water molecules must "hop" several times from one hydration shell to another during the total simulation time, which is in agreement with our observation of headgroup–water bonding times of 1–10 ps for most of the bonded water molecules.

In the interior of the membrane, the diffusion rate increases rapidly upon going toward the middle of the membrane as a result of the larger available free volume (see Figure 5). At the beginning of the tails, at the border of regions 2 and 3, the lipid density is largest. Halfway down the tails the density and free volume are comparable to those of liquid alkanes, and the calculated diffusion coefficient in this part of the membrane is also close to the diffusion coefficient of water in hexadecane (estimated as 12×10^{-5} cm^2/s at 350 K from temperature-dependent diffusion data of Schatzberg[74]). In region 4 the density drops further, and the number of free volume pockets large enough to accommodate a water molecule increases. This facilitates the diffusion process. The same effect, an increasing diffusion rate in regions with lower tail density, has been observed for oxygen

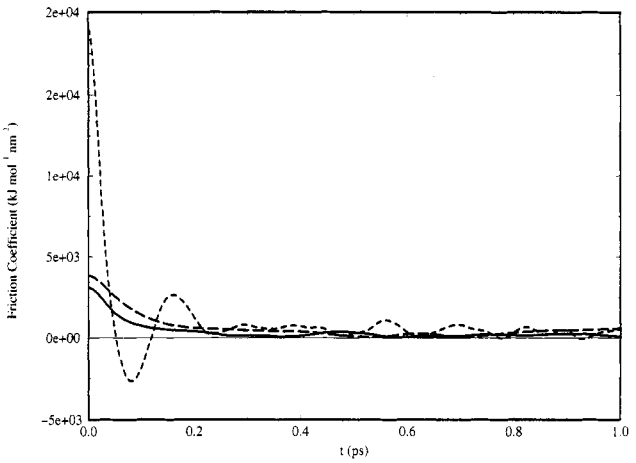

Figure 10. Time-dependent friction coefficient. Dashed curve is computed in region 3, solid curve in region 4, and the long-dashed curve in between.

diffusion through a hexadecane monolayer[5] as well as for the diffusion of benzene in a lipid bilayer.[6]

The difference between the diffusion process in the high- and low-density regions is illustrated in Figure 10. Here we plotted the time-dependent local friction coefficient (eq 33). In the high-density region, the forces are large and the decay time is short, indicating a high local viscosity. The negative correlation at short times results from a backscattering of the penetrant in the micro cavity formed by the lipid surroundings. In the low-density region this behavior is not observed, and the forces are much smaller with a larger decay time.

We also computed the diffusion of water parallel to the membrane (in the xy plane), from the MSD of free water molecules in regions 1 and 2 and of constrained ones in regions 3 and 4. The lateral diffusion profile turned out to be very similar to the perpendicular one, which indicates that on the local scale of diffusion the membrane looks essentially isotropic. This has also been concluded from fluorescence experiments of oxygen diffusion through membranes.[75] Only in region 3 we found a statistically significant difference between the diffusion in z and xy directions, the z diffusion rate being somewhat higher. Here the alignment of the tails is predominantly in the z direction. It is therefore likely that the available free volume is also aligned parallel to the tails. This connectivity of free volume in the z direction might explain the observed larger diffusion rate. Note, however, that diffusion in the xy plane of a z-constrained particle may differ from that of a free particle. The real lateral diffusion rate in regions 3 and 4 may therefore be somewhat higher than observed.

F. Analysis of the Permeation Rate. Knowing the free energy and the diffusion rate as a function of position in the membrane, it is possible to calculate the permeation rate of water using eqs 17 and 20. Integrating from the middle of one water layer to the other, we find $P = 7(\pm 3) \times 10^{-2}$ cm/s. To compare this value with experimentally determined permeation rates, we have to make a temperature correction, since most experiments are performed at lower temperatures (typically around 320 K) than our simulation (350 K). We assume that the temperature dependence of the permeation process is Arrhenius-like. The height of the activation energy for the total permeation process (i.e., diffusion and solubility activation energy) in membranes is far from clear, however. Values derived from temperature-dependent measurements range from 35[76] to 57 kJ/mol.[9] Using an intermediate value of 45 kJ/mol, we estimated the following experimental permeabilities of water through a (liquid-crystalline) DPPC membrane at 350 K: 2.5×10^{-3},[9] 9×10^{-3},[10] and 2.5×10^{-2} cm/s.[11] Through egg-pc values of 3.3×10^{-2},[12] $\sim 7 \times 10^{-2}$,[13] and 4.4×10^{-2} cm/s[14] are obtained after temperature correction, and for the basal permeability through an RBC membrane, 8×10^{-2} cm/s.[15] Considering the wide range of experimental data

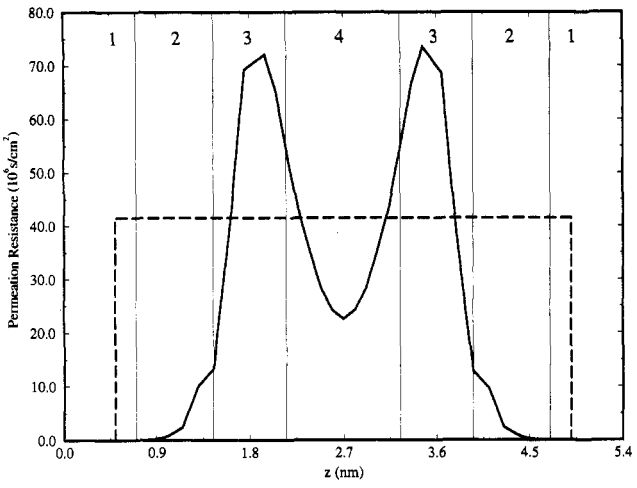

Figure 11. Resistance to permeation. Solid curve is computed from our simulations, and dashed curve is as predicted from the solubility–diffusion model. The middle of the water layer corresponds to $z = 0.0$ and $z = 5.4$. Vertical lines indicate different regions.

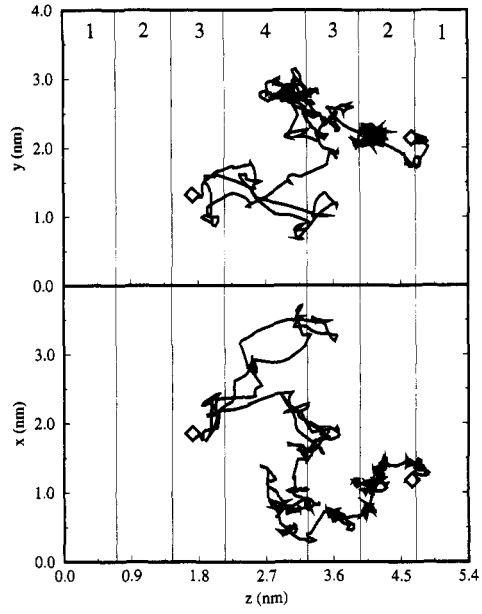

Figure 12. Projection of a typical trajectory of a free water molecule. The upper figure is a projection in the *yz* plane and the lower figure in the *xz* plane. Squares mark the initial (inserted) and final (after 20 ps) positions. The middle of the water layer corresponds to $z = 0.0$ and $z = 5.4$. Vertical lines indicate different regions.

and the uncertainty in the temperature conversion, our value seems reasonable. It definitely supports the idea of a fast permeation rate of water.

In Figure 11 the local resistance to permeation (i.e., the integrand of eq 20) is plotted, together with the equivalent for the homogeneous solubility–diffusion model (eq 10). Although the total area beneath both curves is similar (and thus the predicted permeation rate), it is obvious that the two curves are very dissimilar. Whereas in the solubility–diffusion model the resistance along the bilayer does not change at all, from our simulation it is clear that region 3, the dense part of the hydrocarbon interior, contributes most to the resistance. Due to the larger local diffusion rate, permeation through the middle part of region 4 is relatively easier. Although the diffusion rate in the interfacial region is low, its resistance to permeation is negligible since the shape of the permeation integral is largely determined by the free energy barrier. The overestimation of the self-diffusion rate in the SPC model with respect to the experimental value therefore will have a negligible influence on the total permeation rate. Defining an "effective" distance for water permeation as the width of the part of the membrane that has the main resistance to permeation, we find a rather small value of 2.2 nm. This is only half the value of the total membrane thickness which is used in the homogeneous solubility–diffusion mechanism!

G. Unconstrained Water Molecules. Thus far, the permeation process has been analyzed in terms of an inhomogeneous solubility–diffusion model using the results of restrained MD simulations. As already explained in the Introduction, it would have been impossible to derive the permeation process from normal equilibrium MD simulations. The excess free energy for water in region 4 with respect to the bulklike water in region 1 means that one would expect on average to have 0.2 water molecules solvated into region 4, which is indeed too low to be studied in a statistically significant way. In an extended simulation of our previous, unperturbed system (without inserted water molecules), one water molecule managed to escape into the middle of the membrane. After 10 ps it diffused back to the interface where it came from. Considering the total simulation time of 120 ps, this means an average presence of almost 0.1 water molecule, which is of the right order of magnitude.

The observation of the diffusion of unconstrained water molecules in the membrane interior can be helpful in clarifying the permeation process. Therefore, we decided to do some additional simulations in which an unconstrained water molecule was inserted into the membrane. From this we got several trajectories of the diffusional motion of water molecules in the membrane. Although no quantitative data can be derived from these trajectories, it shows very nicely the character of the diffusion process in the different regions in the membrane. A representative trajectory is plotted in Figure 12. The first thing to notice is that the motion of the water molecule really is diffusive in all parts of the membrane. This is what we already expected based on the correlation times of the random forces (subsection E). Furthermore, Figure 12 indicates that the diffusional jumps are quite large in region 4, where relatively large free volume pockets occur. In region 3 the smaller pockets force the jumps also to be somewhat smaller. Finally, in region 2, the water molecule has become bound to charged interfacial atoms and the diffusion rate is even lower.

6. Discussion

A. Complexity of the Permeation Barrier. The results presented in this work show that the structure and dynamics of a phospholipid membrane differ considerably from that as assumed by the homogeneous solubility–diffusion model. This is due to the inhomogeneous nature of the membrane, which differs considerably from a two-phase water/alkane or water/polymer system. The application of the homogeneous solubility–diffusion mechanism to a lipid membrane therefore seems to be only a first approximation of the real process. Any quantitative predictions based on this model need to be questioned. The complexity of a lipid membrane appears from a variety of observations. First, there is no well-defined boundary present between the water and hydrocarbon phases. Instead, we observe a very rough interface with lipid headgroups pointing into the water layer and strands of water molecules penetrating the membrane, so-called transient defects.[43] Second, the free volume distribution exhibits a large position dependency. The resemblance with a liquid alkane seems to hold only for a small part of the tail region. Third, the approximation of the solubility of water in the membrane by a step function does not correspond to the shape of the free energy profile. Fourth, also the diffusion coefficient varies considerably (more than 1 order of magnitude) along the bilayer normal. The permeation integral clearly shows the differences between the homogeneous solubility–diffusion mechanism and our results.

B. Permeation Described by the Four-Region Model. In our view, a better description of the permeation process can be given within the framework of the "four-region" model, which takes into account the inhomogeneity of the membrane.

Region 1: *Perturbed Water*. This region seems to be the least important for the permeation process. The properties of water molecules in this region remain rather close to the values for bulk water. As can be seen from the presented figures, both the diffusion and the free energy profile remain relatively unchanged. One could therefore only speak of *perturbed* water in this region. These perturbations extend approximately 1.0 nm into the water layer.[61] Although these perturbations are important in the field of hydration forces between membranes,[77,78] it is not very likely that this region plays an important role in the permeation process. Only in the presence of an electrical double layer of ions may an additional resistance to permeation exist, as is observed in experimental studies ("unstirred layer effect").

Region 2: *Bound Water*. In this region there is no longer bulklike water present. Almost all water is *bound* to one or more lipid headgroup atoms in order to replace the missing hydrogen bonds to neighboring water molecules. Diffusion takes place together with the lipids (which diffuse much slower) or as "hopping" from one hydration shell to another which involves the (also slow) process of breaking strong hydrogen bonds. As a result, the diffusion coefficient drops almost an order of magnitude. A consequence of the higher lipid density and the breaking up of the favorable water–water hydrogen bonding network is the increase of the excess free energy with approximately 10 kJ/mol in this region.

Region 3: *High Viscosity*. In this region, almost no more water molecules are present. Entering this region means that the last remaining hydrogen bond with other water molecules has to be broken. The only possibility to maintain favorable short-range electrostatic interactions is offered by the presence of carbonyl groups. The permeation process in this region takes place via singly dispersed water molecules. Due to the high tail density, the membrane behaves as a fluid with *high viscosity*. The water-accessible free volume is small, and a backscattering of the water molecule in its free volume pocket is observed. The diffusion rate is much lower than in liquid alkanes. Low free volume, reduced possibilities for hydrogen bonding, and decreasing electrostatic interactions also result in a strong increase in free energy with about 15 kJ/mol over this region. Both the low diffusion rate and the increase in free energy cause this region to be the main resistance to the permeation of water and probably also for other small molecules.

Region 4: *Low Viscosity*. In this region the lipid density is much lower than in region 3. The tails are much more disordered and create free volume pockets large enough to accommodate water molecules. The diffusion process is characteristic for diffusion in liquids with *low viscosity*, and therefore the diffusion rates are much faster. The excess free energy remains fairly constant, 25 kJ/mol with respect to bulk water. The total excess free energy is too high to allow for a measurable steady water concentration.

The total permeation process of water through the membrane thus can be summarized as follows. It is essentially determined by the free energy barrier that results from the breakage of interwater hydrogen bonds and the loss of electrostatic interactions. The real permeation process starts from the edges of strands of water molecules that already penetrate the membrane quite deeply. After having gained enough energy from random collisions to escape from these strands, the permeation is then mainly limited by diffusion across the highly viscous part of the membrane. The permeation across the middle part is relatively easy. The other side of the membrane offers the same resistance.

The same permeation process might apply to other small, uncharged permeants as well. Additional simulations (e.g., with oxygen and ammonia) are currently being performed to see to what extent the hydrophobicity and the size of the permeants influence the permeation process. It is for instance not immediately clear from which region the special size dependency of the permeation process originates. The high-viscosity region seems to be the best candidate for this role, and this region could then be identified as the experimentally observed non-Stokesian region.[20] In this respect, an analysis of the size and shape distribution of free volume pockets in each of the four different regions will be helpful. After finishing these studies, we hope to present a full picture of the basal permeation process of small molecules through a lipid membrane. In addition, we are also currently investigating the possibility of fast proton transport through transient hydrogen-bonded water chains extending over the full width of the membrane.

C. Sources of Systematic Error. In the computational method that we applied to study the permeation of water, there are several possible sources of systematic error which require some additional discussion. First, let us reconsider one of the assumptions that is made in the theoretical derivation of the permeation process, i.e., that the thermodynamic potential can be considered constant over the correlation distance of the particle. The largest gradient (~ 15 kJ mol^{-1} nm^{-1}) is found in region 3. The largest correlation time in this region was found to be of the order of 0.5 ps. From the highest local diffusion rate in region 3, the correlation distance is then calculated to be only $\sim 5 \times 10^{-3}$ nm. Across such a small distance a gradient of less than 0.1 kJ/mol is expected, which is much smaller than kT, the driving energy of Brownian diffusion. Another way of looking at this is to compare the correlation time in this region with the time scale set by the frequency of the inverted free energy barrier. Approximating the inverted free energy barrier by a harmonic potential, we calculated a frequency of 2×10^{14} Hz (50 ps period), much slower than the correlation time of the forces. This means that we still are in the limit of overdamped Markovian dynamics, implying a diffusive kind of motion across the free energy barrier. Therefore, eq 34 remains a valid approximation.

Apart from the usual uncertainties about force field parameters, two aspects may be of special importance to the water permeation process. The first aspect is the overestimation of the self-diffusion rate in the SPC model with respect to the experimental value. As a consequence, the computed value of the permeation resistance in region 1 (and eventually also in region 2) will be underestimated. However, since the total permeation resistance is mainly determined by regions 3 and 4, this will have a negligible influence on the total permeation rate. The modeling of the hydrocarbon chains as united atoms is another force field approximation which could in principle influence the results of the simulation. One would argue that the diffusion rate will become lower upon explicitly modeling the hydrogen atoms; the locally enhanced roughness will hinder the passage of water molecules. Moreover, a small dipole moment along the C–H bonds could be introduced, resulting in an increased diffusion barrier. Although the effects would probably remain small, they would result in a decrease of the total permeation rate, bringing it closer to most of the reported experimental values.

In order to attain a stable liquid-crystalline phase, the temperature of the simulation was set to the rather high value of 350 K, which is well above the phase transition temperature of the system (315 K). An advantage of the higher temperature is that the phase space of the system can be sampled faster. A drawback, however, is that most experimental measurements of the water permeation are done at lower temperatures. In order to compare the experimental permeation rate with the computed one, we made a temperature correction to the experimental data. The assumption of an Arrhenius type of temperature dependence is the most natural one, but the height of the activation energy barrier is not well determined. Taking the lowest reported value[76] of 35 kJ/mol instead of intermediate value of 45 kJ/mol as we did, the corrected experimental permeation rates to 350 K become on average almost 1 order of magnitude lower. On the other hand, taking the highest value[9] of 57 kJ/mol, the opposite occurs; i.e., the experimental values become an order of magnitude higher. Therefore, a more careful comparison between the computed and experimental permeation rates can only be made once the height of the activation energy barrier is determined more

accurately. Our results correspond to an activation barrier in the order of 50 kJ/mol.

7. Conclusion

We have shown that it is quite feasible to study a slow mechanism as water permeation through a lipid membrane by relatively short MD simulations. From our simulations it is obvious that a straightforward homogeneous solubility–diffusion mechanism is not adequate to describe the permeation of water through a lipid membrane. Treating the membrane as a well-defined two-phase system like alkane/water is definitely an oversimplification. A better way to describe the permeation process through the membrane is using a *four-region model*. This model contains the necessary details to understand the process qualitatively. Quantitative results are obtained by calculating the excess free energy as well as the diffusion rate of water in the membrane as a function of position along the bilayer normal. We computed the permeation rate for water to be $7(\pm 3)\times 10^{-2}$ cm/s at 350 K, close to the permeation rate obtained from experimental measurements. The permeation rate is essentially controlled by the free energy barrier, across which a diffusive kind of motion takes place. The rate-limiting step is the permeation of the water molecule through the dense part of the lipid tail region.

Acknowledgment. This work was supported by the Foundation for Biophysics and the Foundation for National Computer Facilities under the auspices of the Netherlands Organization for Pure Research, NWO. The simulations were performed on the Cray-YMP at the Computing Center of Amsterdam.

References and Notes

(1) Finkelstein, A. *J. Gen. Physiol.* **1976**, *68*, 127.
(2) Finkelstein, A. *Current Topics in Membranes and Transport*; Academic Press: New York, 1984; Vol. 21, pp 295–308.
(3) Potts, R. O.; Francoeur, M. L. *Proc. Natl. Acad. Sci. U.S.A.* **1990**, *87*, 3871.
(4) Jansson, T.; Illsley, N. *J. Membr. Biol.* **1993**, *132*, 147.
(5) McKinnon, S. J.; Whittenburg, S. L.; Brooks, B. *J. Phys. Chem.* **1992**, *96*, 10497.
(6) Bassolino-Klimas, D.; Alper, H. E.; Stouch, T. R. *Biochemistry*, in press.
(7) Egberts, E. Molecular Dynamics Simulation of Multibilayer Membranes. Thesis, University of Groningen, 1988; Chapter 4.
(8) Egberts, E.; Marrink, S. J.; Berendsen, H. J. C. *Eur. Biophys. J.* **1994**, *22*, 423.
(9) Carruthers, A.; Melchior, D. L. *Biochemistry* **1983**, *22*, 5797.
(10) Andrasko, J.; Forsén, S. *Biochem. Biophys. Res. Commun.* **1974**, *60*, 813.
(11) Graziani, Y.; Livne, A. *J. Membr. Biol.* **1972**, *7*, 275.
(12) Finkelstein, A.; Cass, A. *J. Gen. Physiol.* **1968**, *52*, 145s.
(13) Huang, C.; Thompson, T. E. *J. Mol. Biol.* **1966**, *15*, 539.
(14) Fettiplace, R. *Biochim. Biophys. Acta* **1978**, *513*, 1.
(15) Benga, G.; Pop, V. I.; Popescu, O.; Borza, V. *J. Biochem. Biophys. Methods* **1990**, *21*, 87.
(16) Illsley, N. P.; Verkman, A. S. *J. Membr. Biol.* **1986**, *94*, 267.
(17) Verkman, A. S.; Dix, J. A.; Seifter, J. L. *Am. J. Physiol.* **1985**, *248*, F650.
(18) Verkman, A. S.; Ives, H. E. *Am. J. Physiol.* **1986**, *250*, F633.
(19) van Heeswijk, M. P. E.; van Os, C. H. *J. Membr. Biol.* **1986**, *92*, 183.
(20) Garrick, R. A.; Ryan, U. S.; Bower, V.; Cua, W. O.; Chinard, F. P. *Biochim. Biophys. Acta* **1993**, *1148*, 108.
(21) Hanai, T.; Daydon, D. A. *J. Theor. Biol.* **1966**, *11*, 1370.
(22) Finkelstein, A.; Cass, A. *Nature* **1968**, *52*, 145.
(23) Träuble, H. *J. Membr. Biol.* **1971**, *4*, 193.
(24) Graham, T. *Philos Mag.* **1866**, *32*, 401.
(25) Zaccai, G.; Blasie, J. K.; Schoenborn, B. P. *Proc. Natl. Acad. Sci. U.S.A.* **1980**, *72*, 376.
(26) Levine, Y. K.; Wilkins, M. H. F. *Nature New Biol.* **1971**, *230*, 89.
(27) Damadoran, K. V.; Merz, K. M.; Gaber, B. P. *Biochemistry* **1992**, *31*, 7656.
(28) Damadoran, K. V.; Merz, K. M. *Langmuir* **1993**, *9*, 1179.
(29) Heller, H.; Schaefer, M.; Schulten, K. *J. Phys. Chem.* **1993**, *97*, 8343.
(30) Stouch, T. R. *Mol. Simulat.* **1993**, *10*, 335.
(31) Lieb, W. R.; Stein, W. D. *Nature* **1969**, *224*, 240.
(32) Lieb, W. R.; Stein, W. D. *Curr. Top. Membr. Transp.* **1971**, *2*, 1.
(33) Walter, A.; Gutknecht, J. *J. Membr. Biol.* **1986**, *90*, 207.
(34) Fujita, H. *Fortschr. Hochpolym. Forsch.* **1961**, *3*, 1.
(35) Vrentas, J. S.; Duda, J. L. *Macromolecules* **1976**, *9*, 785.
(36) Cohen, M. H.; Turnbull, D. *J. Chem. Phys.* **1959**, *31*, 1164.
(37) Tam, C. M.; Matsuura, T.; Tremblay, A. Y. *J. Colloid Interface Sci.* **1991**, *147*, 206.
(38) Takeuchi, H.; Okazaki, K. *Macromol. Chem., Macromol. Symp.* **1993**, *65*, 81.
(39) Sok, R. M.; Marrink, S. J.; Berendsen, H. J. C. Manuscript in preparation.
(40) Nonnenmacher, T. F. *Eur. Biophys. J.* **1989**, *16*, 375.
(41) Stauffer, D.; Aharony, A. *Introduction to Percolation Theory*; Taylor & Francis: London, 1992.
(42) Fettiplace, R.; Haydon, D. A. *Physiol. Rev.* **1980**, *60*, 510.
(43) Deamer, D. W.; Bramhall, J. *Chem. Phys. Lipids* **1986**, *40*, 167.
(44) Weaver, J. C.; Powell, K. T.; Mintzer, R. A.; Sloan, S. R.; Ling, H. *Bioelectrochem. Bioenerg.* **1984**, *12*, 405.
(45) Levitt, D. G. *Biochem. Biophys. Acta* **1974**, *373*, 115.
(46) Schulten, K.; Schulten, Z.; Szabo, A. *J. Chem. Phys.* **1981**, *74*, 4426.
(47) Berendsen, H. J. C.; Postma, J. P. M.; van Gunsteren, W. F.; Dinola, A.; Haak, J. R. *J. Chem. Phys.* **1984**, *81*, 3684.
(48) van Gunsteren, W. F.; Berendsen, H. J. C. *Groningen Molecular Simulation (GROMOS)*; software package, Biomos, Nijenborgh 4, 9747 AG Groningen, The Netherlands.
(49) Berendsen, H. J. C.; Postma, J. P. M.; van Gunsteren, W. F.; Hermans, J. *Intermolecular Forces*; Pullman, B., Ed.; Reidel: Dordrecht, 1981; pp 331–342.
(50) van Buuren, A. R.; Marrink, S. J.; Berendsen, H. J. C. *J. Phys. Chem.* **1993**, *97*, 9206.
(51) Widom, B. *J. Chem. Phys.* **1963**, *39*, 2802.
(52) Hermans, J.; Pathiaseril, A.; Anderson, A. *J. Am. Chem. Soc.* **1988**, *110*, 5982.
(53) Shing, K. S.; Gubbins, K. E. *Mol. Phys.* **1982**, *46*, 1109.
(54) Allen, M. P.; Tildesley, D. J. *Computer Simulation of Liquids*; Oxford University Press: Oxford, 1987.
(55) Roux, B.; Karplus, M. *J. Phys. Chem.* **1991**, *95*, 4856.
(56) Kubo, R. *Rev. Mod. Phys.* **1966**, *29*, 255.
(57) Ciccotti, G.; Jacucci, G. *Phys. Rev. Lett.* **1975**, *35*, 789.
(58) Bondi, A. *J. Phys. Chem.* **1954**, *58*, 929.
(59) A copy of a 10-min video film can be obtained for U.S. $40, from BIOMOS bv, Nijenborgh 4, 9747 AG Groningen, The Netherlands.
(60) Casal, H. L. *J. Phys. Chem.* **1989**, *93*, 4328.
(61) Marrink, S. J.; Berkowitz, M.; Berendsen, H. J. C. *Langmuir* **1993**, *9*, 3122.
(62) Borle, F.; Seelig, J. *Biochim. Biophys. Acta* **1983**, *735*, 131.
(63) Lundberg, B.; Svens, E.; Ekman, S. *Chem. Phys. Lipids* **1978**, *22*, 285.
(64) Finer, E. G.; Darke, A. *Chem. Phys. Lipids* **1974**, *12*, 1.
(65) Seelig, A.; Seelig, J. *Biochemistry* **1974**, *13*, 4839.
(66) Seelig, J.; Seelig, A. *Q. Rev. Biophys.* **1980**, *13*, 19.
(67) Marqusee, J. A.; Dill, K. A. *J. Chem. Phys.* **1986**, *85*, 434.
(68) Schatzberg, P. *J. Phys. Chem.* **1963**, *67*, 776.
(69) Postma, J. P. M. A Molecular Dynamics Simulation of Water. Thesis, University of Groningen, 1985.
(70) Wu, E.; Jacobson, K.; Papahadjopoulos, D. *Biochemistry* **1977**, *16*, 3936.
(71) Vaz, W. L. C.; Stümpel, J.; Hallman, D.; Gambacorta, A.; De Rosa, M. *Eur. Biophys. J.* **1987**, *15*, 111.
(72) Fahye, P. F.; Webb, W. W. *Biochemistry* **1978**, *17*, 3046.
(73) Rubinstein, J. L. R.; Smith, B. A.; McConnell, H. M. *Proc. Natl. Acad. Sci. U.S.A.* **1979**, *76*, 15.
(74) Schatzberg, P. *J. Polym. Sci.* **1965**, *10C*, 87.
(75) Fishkoff, S.; Vanderkooi, J. M. *J. Gen. Physiol.* **1975**, *65*, 663.
(76) Reeves, J. P.; Dowben, R. M. *J. Membr. Biol.* **1970**, *3*, 123.
(77) Marcelja, S.; Radic, N. *Chem. Phys. Lett.* **1976**, *42*, 129.
(78) Rand, R. P.; Parsegian, V. A. *Biochim. Biophys. Acta* **1989**, *988*, 351.